Magazine of Concrete Research, 1994, **46**, No. 167, June, 133–143

A generalized lower-bound analysis of anchorage zones

T. J. Ibell* and C. J. Burgoyne*

UNIVERSITY OF CAMBRIDGE ENGINEERING DEPARTMENT

This Paper is the last of three on the behaviour of anchorage zones for prestressed concrete. Details of a lower-bound approach to the ultimate load analysis of concrete prisms strip-loaded through rigid steel plates are presented. The previous papers of the series presented experimental results and analytical plasticity solutions to this problem. This Paper extends the plasticity solution by using a finite element approach, thus enabling three-dimensional failure mechanisms encountered during the experiments to be studied successfully. The analysis is conducted in two stages: the first to determine the cracked state of the anchor block; the second to determine the final failure load. It is shown that such an approach is useful in the design of anchorage zones for prestressed concrete.

Notation

a	half-breadth of test specimens
a_1	half-length of loading plate
a_1/a	concentration ratio
A_s	total area of reinforcing steel crossing a plane
c_c	cohesion of the concrete
D_r	depth of reinforcement
E_c	Young's modulus for concrete
f_c	'effective' concrete compressive strength
f'_c	concrete cylinder compressive strength
f_{cu}	concrete cube compressive strength
f_t	'effective' concrete tensile strength
f'_t	concrete split-tensile strength
f_y	yield strength of steel reinforcing bars
h	height of concrete prism
k	factor to cause sliding failure for a particular stress state
k_{tens}	factor to cause tensile failure for a particular stress state
L	length of central crack
P	applied ultimate load capacity
P^*	predicted ultimate load capacity
P^*_{all}	predicted ultimate load capacity with all steel assumed yielded
$P^*_{2\cdot4a}$	predicted ultimate load capacity with steel yielding to depth $2\cdot4a$
P^*_{wedge}	predicted ultimate load capacity with steel yielding over depth of wedge
R	radius of Mohr's circle for any stress state
R'	radius of Mohr's circle at failure
T	total tensile force exerted by the steel reinforcement
w	width of test specimens
x, y, z	axis labels
β	half-wedge failure angle (to the vertical)
ν	'effectiveness factor' for concrete
ν_t	'tensile effectiveness factor' for concrete
$[\sigma]$	full stress state along a wedge plane
$[\bar{\sigma}]$	average stress state on a wedge plane
$\sigma_1, \sigma_2, \sigma_3$	principal stresses
σ_c	centre of Mohr's circle of stress
$[\bar{\sigma}]_P$	average stress state on a wedge plane due to applied load
$[\bar{\sigma}]_S$	average stress state on a wedge plane due to steel forces
ϕ	internal angle of friction of concrete
Φ	steel parameter

Introduction

In a previous paper,[1] tests on centrally strip-loaded concrete prisms and their failure mechanisms were

* University of Cambridge.
Paper received 27 June 1993.

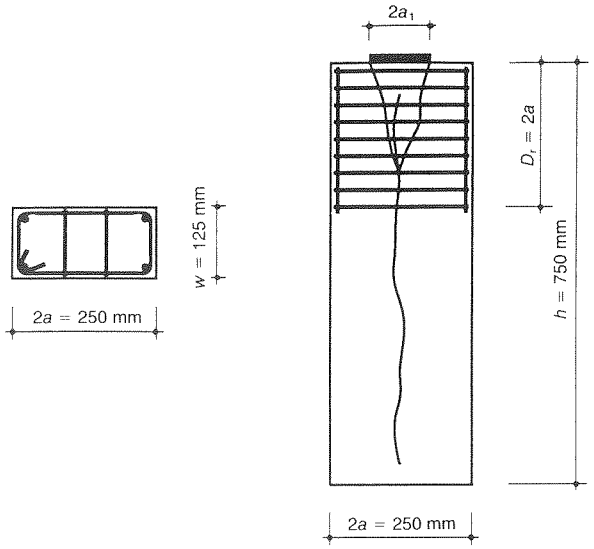

Fig. 1. Arrangement of the test specimens, showing typical steel reinforcement and final wedging failure

reported in some detail. It was found that, in general, failure of these strip-loaded prisms occurred in a two-step process. Initial central cracking, extending nearly the full length of the specimens, preceded planar wedge formation beneath the loading plate. Fig. 1 shows the overall loading arrangement, steel reinforcement layout and general wedging failure mechanism of the test specimens of Ref. 1. The present problem can thus be considered as a case of shearing along yield lines at failure. Although good agreement was obtained by using plasticity theory in an analysis described in a subsequent paper,[2] it was decided to formulate a generalized lower-bound solution to the problem for two main reasons.

(*a*) The analytical solutions presented before take no account of the out-of-plane (three-dimensional (3-D)) nature of failure of the strip-loaded specimens for high reinforcement ratios.[1] These solutions were found to deviate progressively from the test results as the amount of steel increased.[3]
(*b*) The presence of ducts (and possibly flanges) cannot be modelled adequately by these simple planar methods.

It was therefore decided to incorporate the use of finite element (FE) analysis in the lower-bound solution, for the following reasons.

(*a*) The full stress condition along the failure plane would be known, so that a more general failure criterion could be applied to the wedge. Out-of-plane failure[1] could also be studied.
(*b*) It would be possible to incorporate a beam support in the region of the anchorage zone to determine its effect on the bursting stresses (this is not described in this Paper). In addition, the effect of the presence of a duct in the anchorage zone could be studied.

In addition to the decision to use FEs, it was necessary to consider the use of linear or non-linear types of analysis.

Observation of the experiments had shown that a definite two-step failure mechanism existed for the prisms. A central crack was initiated, and propagated until wedge failure occurred under the loading plate. It was therefore decided to separate the problem into these two stages, each being represented by a linear elastic analysis. Not only was this deemed to be sufficiently representative of the failure mechanism, but it also promised a simplified analysis technique. Use of a linear analysis also brings the method within the capability of most design offices, which cannot justify the cost and complexity of non-linear analysis programs.

Failure model

The analysis is conducted in two distinct stages. In the first case, the whole of the region of interest is modelled by linear elastic FEs, and subjected to an unfactored applied load. From the *pattern* of stresses that result in the concrete the engineer determines *where* the concrete will crack, and from the *magnitude* of the stresses determines at what load the structure will crack.

The structure is then remodelled, with boundaries between elements being placed at the crack positions, and with no connection across the crack. The presence of steel across the crack will be considered later by applying forces across the crack, but no attempt will be made to apply any kinematic boundary conditions.

The structure is then analysed twice, once with just the applied loads and again with just the steel forces. These are then combined linearly, and the stresses across potential failure planes are considered, to get an estimate of the final failure load.

This method does not attempt to follow the full response of the structure to the applied loads: this is not of much interest to the design engineer. What is important is that a reasonable estimate be made of the serviceability limit (first cracking) and the ultimate load. This Paper concentrates on the second stage of the analysis; the first stage is mentioned briefly.

Analysis to determine cracking load

Cracking is assumed to have occurred centrally at the load at which the split-tensile strength of the concrete is reached (from a linear elastic FE analysis). If steel reinforcement is present in the specimen, a variation of steel stress is assumed to act across the potential crack plane based on experimental evidence. From the experiments conducted in this study, it was generally found that the average steel strain at *visible* cracking was about 300 $\mu\epsilon$. This information was therefore used directly in the above analyses to determine visible cracking loads of the specimens.

The length of the crack at the time that ultimate wedging failure occurs cannot, of course, be determined from this single analysis. The choice of this crack length is discussed below.

Second-stage analysis

The second phase of the analysis is based on the assumption that when the ultimate load is reached, there must exist a plane (or set of planes) along which the stresses are at limiting values. It is assumed that the geometry of these planes is known, or can be defined by one or more pattern parameters, and that there is some criterion, based on average stresses, for saying that failure is taking place along that plane. It is also assumed that all steel is yielding, so that the forces exerted by the reinforcing steel are known.

The method is illustrated by considering the failure of the prisms tested and analysed elsewhere.[1,2] The pattern parameter used is the angle β, which is defined in Fig. 2, and the concrete failure criterion adopted is the modified Coulomb criterion, which is defined below.

Because the steel forces are fixed but the applied load is unknown, two analyses have to be carried out. They can, however, be done as two separate loading cases on the same set of elements, and are independent of the pattern parameter, which is used only when the results of the two analyses are combined.

Thus, the procedure can be summarized as follows.

(*a*) Apply a standard load (say 1 N/mm^2) to the prism over the loading area and determine from an FE analysis the stress distribution σ_P throughout the region of interest.

(*b*) Apply forces to the prism to represent the steel at yield and determine the stress distribution σ_S over the same area. The actual positioning of the steel forces is not particularly important; they must act along the line of action of each bar (or group of bars) with the correct force, but can be positioned anywhere along that bar provided the bar does not terminate within any zone involved in the failure process.

(*c*) For each value of the pattern parameter β, determine the mean values of the stresses along the failure plane due to the applied load $[\bar{\sigma}]_P$ and the steel forces $[\bar{\sigma}]_S$.

(*d*) Find the proportion of $[\bar{\sigma}]_P$ that must be added to $[\bar{\sigma}]_S$ to give a total stress $[\bar{\sigma}]$ that satisfies the modified Coulomb failure criterion. That proportion then represents the load factor that must be applied to the standard load to cause failure along a plane defined by the specified value of β.

(*e*) Vary β to find the minimum load factor.

Only two (linear) FE runs have to be carried out in order to analyse a particular prism containing any quantity of steel reinforcement or of any concrete strength.

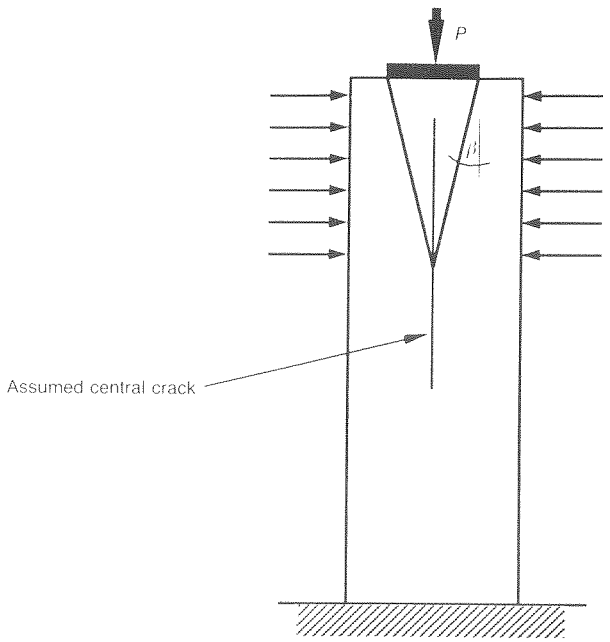

Fig. 2. General model of applied steel forces at ultimate failure of the (reinforced) concrete prisms: horizontal arrows represent applied steel forces under the assumption that steel acts at yield stress f_y at ultimate

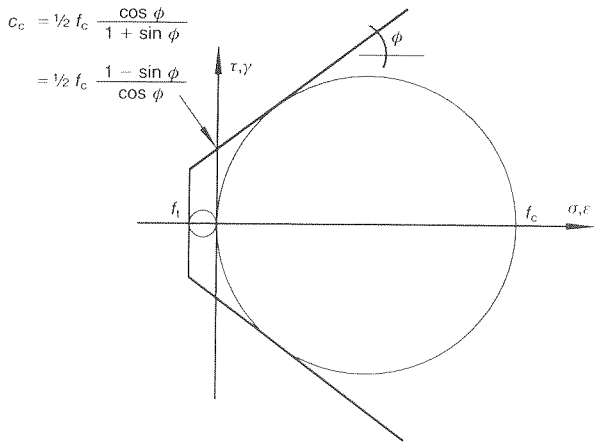

Fig. 3. The modified Coulomb failure criterion, with non-zero tension cut-off

The modified Coulomb failure criterion

Figure 3 shows the modified Coulomb failure criterion envelope for concrete. It can be shown[4] that the cohesion c_c is given by

$$c_c = \frac{1}{2} f_c \frac{(1-\sin\phi)}{\cos\phi} = \frac{1}{2} f_c \frac{\cos\phi}{(1+\sin\phi)} \quad (1)$$

Consider the Mohr's circle of stress (σ_1, σ_3) shown in Fig. 4, which just touches the failure envelope. If

$$\sigma_c = \frac{\sigma_1+\sigma_3}{2} \quad (2)$$

$$R = \frac{\sigma_1-\sigma_3}{2} \quad (3)$$

then simple trigonometry gives

$$c_c \cos\phi = R - \sigma_c \sin\phi \quad (4)$$

Both σ_c and R can be expressed as functions of the applied load factor and the stresses $[\bar{\sigma}]_P$ and $[\bar{\sigma}]_S$; substitution of these results into equation (4) gives a quadratic in the load factor k, which can then be determined.

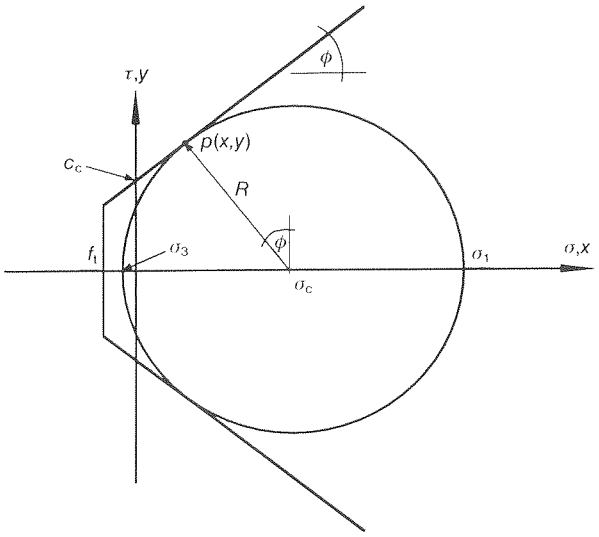

Fig. 4. A failure state of stress, according to the modified Coulomb failure criterion

Failure along the wedge plane may occur by tensile separation if the failure circle shown in Fig. 3 touches the vertical cut-off line at tensile stress f_t. If failure is to occur by separation and not by sliding, then from Fig. 4 the factor k_{tens} to be applied to a state of stress before separation failure occurs is defined as

$$k_{tens} = \frac{-f_t}{\sigma_3} \qquad (5)$$

where f_t is taken as positive in tension and σ_3 is positive in compression.

If k_{tens} is positive and less than k, separation will occur before sliding; otherwise sliding will be the mode of failure. It is now possible to calculate by what factor any given state of stress can be increased before violation of the failure criterion occurs.

Two-dimensional FE models

Initially, several meshes were chosen for the analyses to compare with the test data, but eventually the simple meshes shown in Fig. 5 were found to be sufficiently accurate for all the two-dimensional (2-D) analysis work. Due to symmetry, only half the problem needs to be modelled. Because of the variable size of the loading plate, it is necessary to use different meshes for different a_1/a ratios.

All elements are linear elastic, eight-node quadrilaterals. Both plane stress and plane strain analyses are carried out. The following general assumptions are made throughout the analyses in this Paper.

(*a*) The internal angle of friction for concrete ϕ is a constant 37°.[4]

(*b*) The effectiveness factor ν for the concrete cube compressive strength f_{cu} is taken as 0·67.[5,6]

(*c*) The Young's modulus for the concrete E_c is 28 kN/mm^2 and the Poisson's ratio is 0·17.[7]

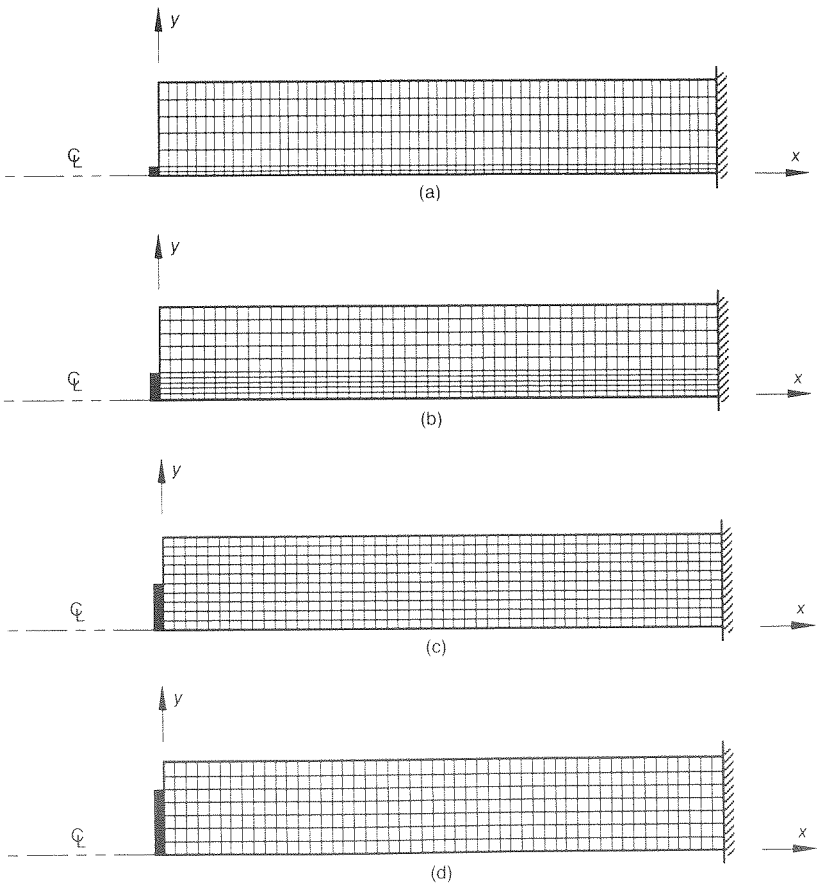

Fig. 5. FE meshes for 2-D analyses: (a) a_1/a = 0·1; (b) a_1/a = 0·3; (c) a_1/a = 0·5; (d) a_1/a = 0·7

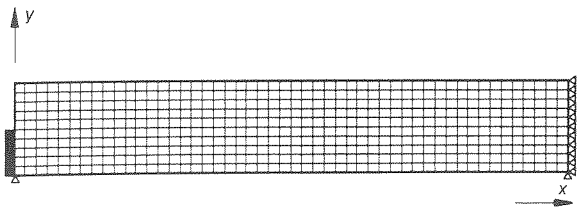

Fig. 6. Fully cracked condition for ultimate analysis

Ultimate failure of unreinforced specimens

The analysis method outlined above is now applied to the determination of the ultimate load capacity of unreinforced specimens under planar wedging. It is assumed that some cracking has occurred in the concrete along the central axis. The stress distribution in the wedging region, and hence the failure load and failure angle, depend on the position and extension of this central crack.

Several step-by-step failure analyses were carried out. A short central crack was assumed over the region most highly stressed in tension. Supports were removed along the centre-line for the specific case of $a_1/a = 0{\cdot}5$ and the prism was reloaded. More supports were removed as the maximum tensile stress concentrated around the crack ends, and it was found that the ultimate failure load dropped slightly with every increase in crack length. It was concluded that this method was unsatisfactory for general use, as the stress concentration around the crack tip was not being modelled accurately.

Since only a lower bound was being sought, it was decided that only one case of central cracking need be considered. The prism was taken to be entirely *cracked* along its length at wedge failure ('fully cracked' condition), as shown in Fig. 6.

Ultimate failure of reinforced specimens

The fully cracked model was also adopted for the analysis of the reinforced specimens. The steel (which is assumed to have yielded) was modelled as applied loads acting on the concrete prism.

Plane strain conditions were chosen for the modelling of this part of the problem in two dimensions. This was considered to be a better approximation to the experiments than plane stress (particularly for low steel reinforcement ratios) because of the confining action provided by the stirrups, cross-links and loading plate.[1]

Figure 7 shows the results of these analyses for the series I (unreinforced) and series III test cases. The latter tests were for samples with cross-links provided to prevent failure in the third direction and to create plane strain conditions.[1] These results showed that the fully cracked condition is suitable for use in this analysis technique. The results are all fairly accurate, except for specimen 0001 (which failed by splitting) and specimens with high reinforcement ratios and low a_1/a ratios (where failure

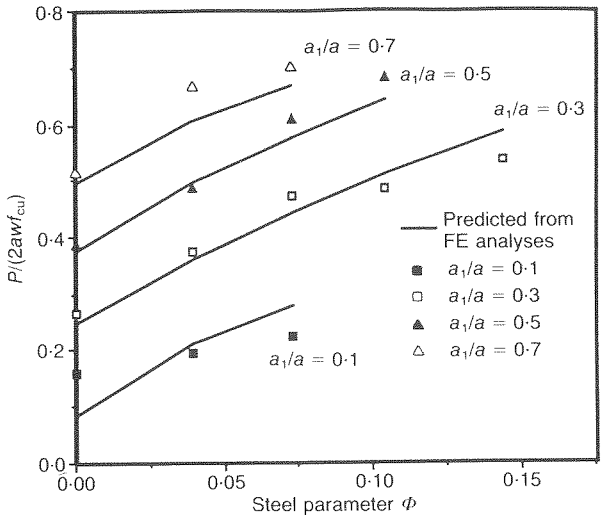

Fig. 7. Predicted ultimate loads for fully cracked condition plotted against series I and III test results

was caused by third-direction wedging and not by the mode assumed in this analysis). It was therefore necessary to study this third-direction failure mode using 3-D FEs as described below. Full details of the specimens, together with their nomenclature, are given in Ref. 1.

Failure angles

Experimental results suggested a fairly constant wedge half-angle β in the concrete of about 14°. The lower-bound method produces angles of failure for the unreinforced specimens ranging from 11° for $a_1/a = 0{\cdot}1$ to 23° for $a_1/a = 0{\cdot}7$. As the amount of steel increases, the predicted failure angles reduce, to a range of 9°–20°. However, from the variation in predicted failure loads with β for any particular specimen, it was found that there existed a fairly flat response to change in β around the actual optimum value of β.

3-D FE meshes

It was considered necessary to model the present problem using 3-D FEs, so that out-of-plane failure could be studied. In order to increase accuracy and minimize the number of elements, linear elastic 20-node brick elements were chosen. Due to symmetry, only one quarter of the problem needs to be modelled (see Fig. 8).

For planar analyses a single layer of elements in the third (z) direction in the model is, of course, sufficient, as shown in Fig. 8. However, to study failure of the specimens in the third direction, the mesh was refined by adding a second layer of elements.

3-D stress analysis

Precisely the same failure model was adopted for the 3-D case as was used previously for the 2-D case. However, there are two differences in the overall analysis of the problems.

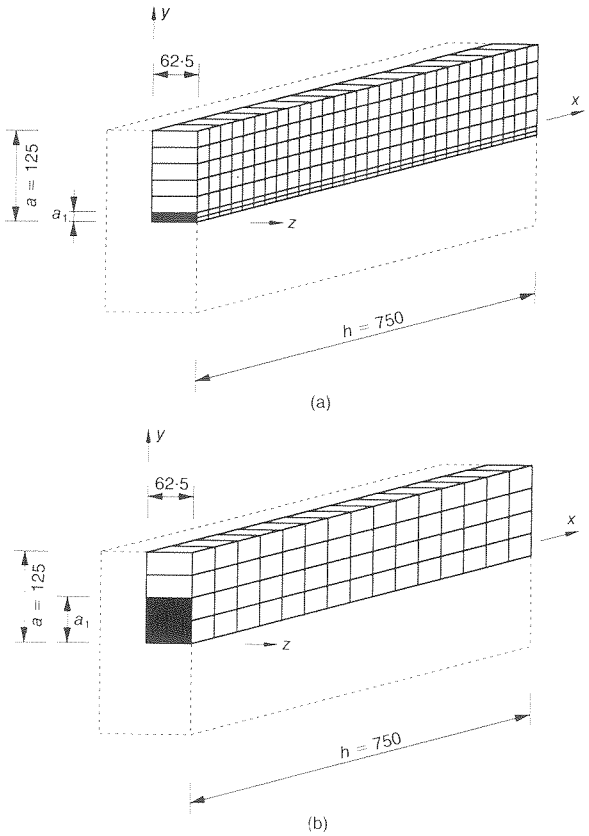

Fig. 8. FE mesh for 3-D analysis of blocks: (a) $a_1/a = 0{\cdot}1$; (b) $a_1/a > 0{\cdot}1$

First, the average stress state along a potential failure plane must be converted into a 3-D Mohr's circle of stress in a manner similar to that described above for the 2-D case.

Second, for 3-D problems, two distinct modes of ultimate failure need to be checked. Failure is either by planar wedging (as assumed in the 2-D case) or by third-direction wedging. The models for these types of failure are shown in Fig. 9. It is assumed that one or the other, but not both, occurs. It is further assumed that, where failure is caused by out-of-plane wedging, only violation of the failure criterion along the *sloped* out-of-plane wedge surface will lead to failure in this direction. The stresses on the other two surfaces of the wedge are ignored entirely in this analysis, because there was very little restraint in the z direction outside the failure zone.

As a check, the 3-D mesh was used to re-analyse one of the planar cases with fully supported edge planes in the z-direction, to give an approximation to the plane strain case. Negligible difference between the two analyses was found.

Ultimate failure of unreinforced specimens (3-D analysis)

Under the assumption that the plate prevents the concrete with which it is in contact from displacing laterally, similar results to those of the plane strain unreinforced analyses were obtained.

Ultimate failure of reinforced specimens (3-D analysis)

In the test specimens, cross-links were positioned between the stirrup legs to tie them together and help maintain plane strain conditions.[1] It was considered necessary to include this steel reinforcement in the 3-D model. However, there was no justification for assuming that such cross-link steel had yielded during planar wedging failure. It was therefore decided to revert to 'plane strain' analyses using 3-D elements, with no out-of-plane movement permitted on the edge planes, to model the problem where cross-links were present. Naturally, the results obtained under these assumptions were similar to those under pure plane strain conditions. This method did, however, allow modelling of the ducted specimens for the first time. Reasonably good correlation was found under this failure analysis, implying that 3-D analysis of ducted specimens could be important.[3]

Out-of-plane wedging failure

To model third-direction failure, it is assumed that a wedge, as shown in Fig. 9(b), is critical. The state of stress along the sloping plane is found and applied to the failure

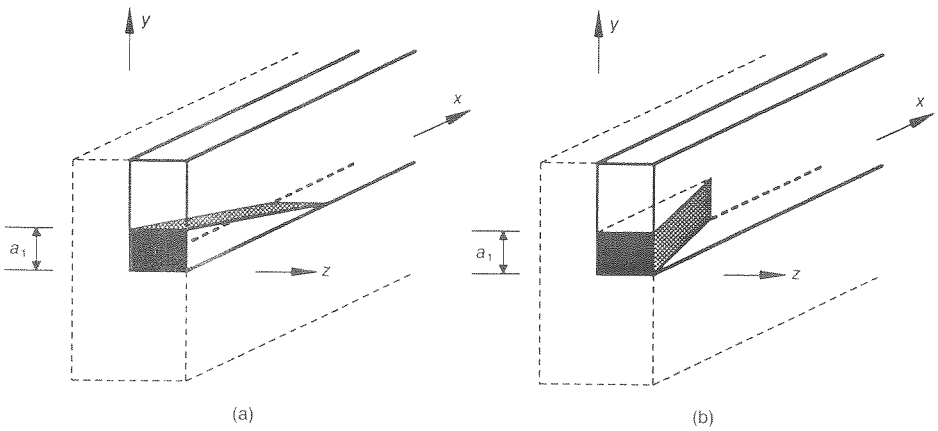

Fig. 9. Wedging failures in (a) the planar mode, (b) the third direction

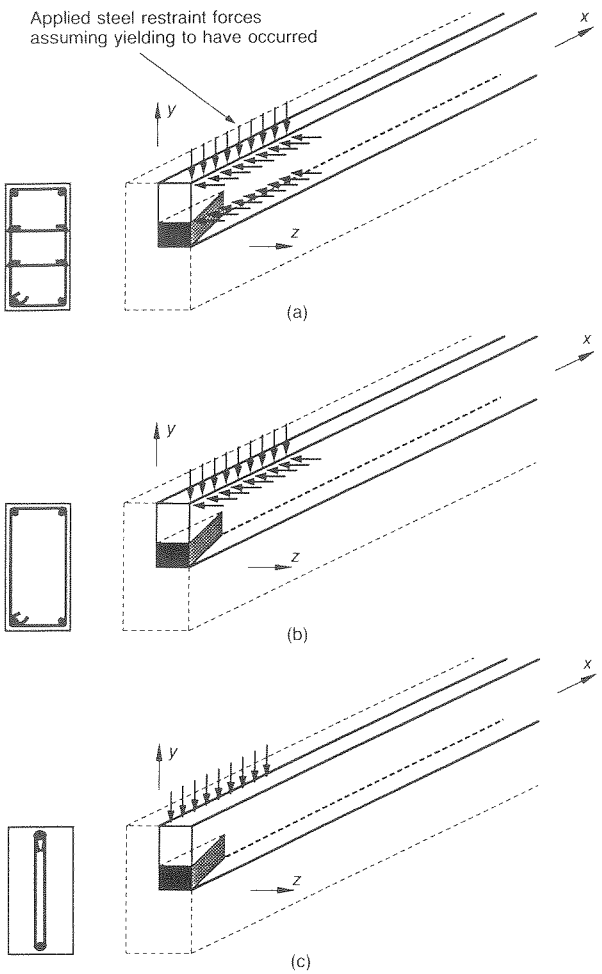

Fig. 10. Models for third-direction failure under various steel arrangements: (a) cross-linked stirrups; (b) no cross-links; (c) central steel

criterion already formulated. A critical wedge is determined on which failure is probable, and the corresponding load capacity is calculated. Where stirrups with cross-links are employed, it is assumed that all steel has yielded across these wedge planes, due to dilatation effects. In addition, the stirrup legs in the third direction are assumed to have yielded in the out-of-plane wedging analyses.

Figure 10 shows the various models used to predict third-direction failure under different steel reinforcement layouts. In all cases, the steel plate is assumed to restrain the concrete, on which it immediately bears, from displacing laterally.

Figure 11 shows predictions of both wedging and third-direction failure for the specimens containing cross-links in the test series. Generally, third-direction failure is predicted to occur for high reinforcement ratios, as found experimentally.

Table 1 gives ultimate load predictions for all test specimens in the present research, from both planar wedging and out-of-plane analyses. Where predicted behaviour is by planar wedging, the fully cracked condition has been assumed. The term 'lower failure' is used to represent failure of the specimens with a_1/a =

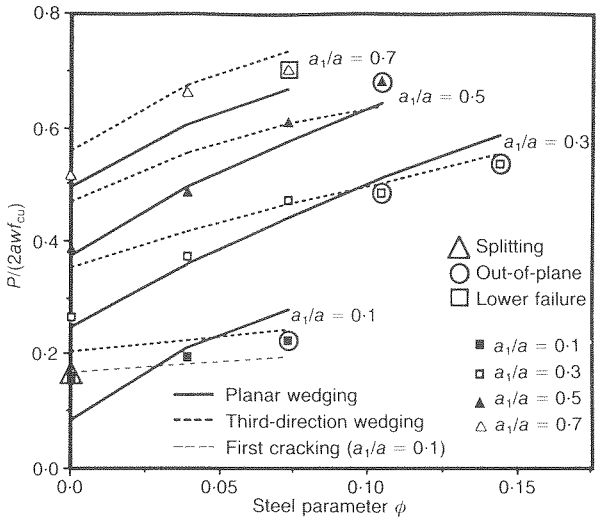

Fig. 11. Theoretical predictions of failure models and capacities for the cross-linked specimens (planar wedging is under the fully cracked assumption)

0·7 which failed, or are predicted to have failed, by crushing of the lower portion of unreinforced concrete. The expected and actual behaviour of each prism is given. Overall correlation is reasonably good, and behaviour predictions are correct in most cases. In general, cases where incorrect behaviour predictions are made occur close to the predicted crossover point from one mode of failure to another.

Comparison of the lower-bound method and existing strip-loading test data

Niyogi[8] carried out several strip-loading tests on unreinforced rectangular concrete prisms of various dimensions. In all cases, he reported planar wedging failure of the prisms, hence only 2-D (plane strain) analyses are carried out here.

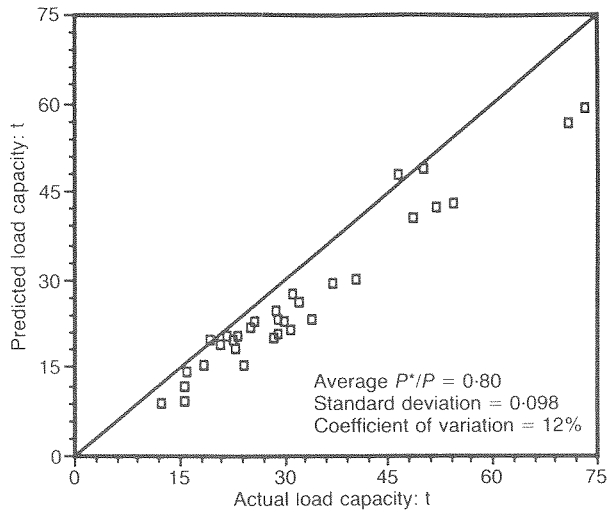

Fig. 12. Correlation of Ref. 8 test results and predictions of the present method of analysis

Niyogi reported the cylinder compressive strength of concrete f'_c for each test. To use these strengths in the present analysis, it was assumed that the cube strength f_{cu} of the concrete is $1{\cdot}25f'_c$. Fig. 12 shows details of the results obtained from 2-D analyses of the prisms. Reasonably accurate modelling of his results has been achieved.

Fenwick and Lee[9] carried out strip-loaded tests on concrete prisms, of rectangular and I-section, as shown in Fig. 13. The prisms were reinforced from the loading plate down to the base, with various quantities of steel reinforcement.

Three-dimensional brick elements were used throughout these analyses. It was felt that this would produce an accurate analysis due to the presence of a duct hole and flanges of the I-section. It is possible that 2-D elements could have been used, with variations in element thickness at points of local geometry change. Because the steel reinforcement was placed so far down the prism, it was not immediately obvious how far down to assume the steel had yielded. Three cases of relevance were therefore considered.

(*a*) Only the steel reinforcement over the wedge length (which has to be found iteratively, as it is not known at the start of the analysis) has yielded. The remaining steel lower down is assumed to have zero stress. (The predicted ultimate load is denoted by P^*_{wedge}).

(*b*) Steel reinforcement over a depth $2{\cdot}4a$ has yielded, and the remaining steel lower down in assumed to have zero stress. This assumption is based on findings from the present experimental test series,[1] in which steel reinforcement was found to yield down to a depth of $2{\cdot}4a$ only. (The predicted ultimate load is denoted by $P^*_{2{\cdot}4a}$.)

(*c*) All the steel is assumed to have yielded. (The predicted ultimate load is denoted by P^*_{all}.)

Table 1. Comparison of all ultimate test results with the present theory

Series	Specimen code	Test load at ultimate P: t	Predicted load at ultimate P: t	Test behaviour†	Predicted behaviour†	P^*/P
I	0001	30	31	S	S	1·03
	0003	50	43	PW	PW	0·86
	0005	72	70	PW	PW	0·97
	0007	96	93	PW	PW	0·97
II	0503-4	69	65	PW	PW	0·94
	1003-4	76	70	OPW	OPW	0·92
	1503-6	78	71	OPW	OPW	0·91
	0505-4	92	92	PW	PW	1·00
	1005-4	111	101	OPW	OPW	0·91
	1505-6	108	102	OPW	OPW	0·94
	0507-4	125	116	PW	PW	0·93
	1007-4	133	118	LF	OPW	0·89
	1507-6	135	120	LF	OPW	0·89
III	0501-4	37	40	PW	PW	1·08
	1001-4	42	44	OPW	OPW	1·05
	0503-4	70·5	67	PW	PW	0·95
	1003-4	88·5	82	PW	PW	0·93
	0503-6	74·5	72	PW	PW	0·97
	1003-6	82	85	OPW	OPW	1·04
	1503-6	90	92	OPW	OPW	1·02
	2003-6	101	104	OPW	OPW	1·03
	0503-2	71	74	PW	PW	1·04
	0505-4	91·5	92	PW	PW	1·01
	0805-4	103	99	PW	PW	0·96
	1005-4	115	105	PW	PW	0·91
	1505-6	128	120	OPW	OPW	0·94
	0505-6	100	96	PW	PW	0·96
	1005-6	107	108	PW	PW	1·01
	0405-2	87	91	PW	PW	1·05
	0307-4	104	105	PW	PW	1·01
	0507-4	124·5	114	PW	PW	0·89
	0807-4	132	123	PW	PW	0·93
	0507-6	127·5	119	PW	PW	0·93
	1007-6	131	122	LF	LF	0·93
	0307-2	108	108	PW	PW	1·00

Table 1 (continued)

Series	Specimen code	Test load at ultimate P: t	Predicted load at ultimate P: t	Test behaviour†	Predicted behaviour†	P^*/P
IV	0503C-4	60·5	67	OPW	PW	1·11
	0505C-4	84·5	91	OPW	OPW	1·08
	0507C-4	110·5	113	OPW	PW/OPW	1·02
V	0003D	49	40	PW	PW	0·82
	0005D	70	66	PW	PW	0·94
	0007D	91·5	88	PW	PW	0·96
	1003D-4	85	82	PW	PW	0·96
	0805D-4	100	98	PW	PW	0·98
	0507D-4	119·5	111	PW	PW	0·93
VI	100316aE-4	73	85	PW	PW	1·16
	080516aE-4	90	101	PW	PW	1·12
	050716aE-4	108	119	PW	PW	1·06
	10033aE-4	84	75	PW	PW	0·89
	08053aE-4	105·5	94	PW	PW	0·89
	05073aE-4	132	110	PW	PW	0·83
	10033aS-4	83	76	PW	PW	0·92
	08053aS-4	101	97	PW	PW	0·96
	05073aS-4	117	112	PW	PW	0·96
	10034aE-4	69·5	70	PW	PW	1·01
	08054aE-4	94	89	PW	PW	0·95
	05074aE-4	114	105	PW	PW	0·92
	10034aS-4	71	72	PW	PW	1·01
	08054aS-4	92	92	PW	PW	1·00
	05074aS-4	107	109	PW	PW	1·02
VII	0001I	22	14	PW	PW	0·64
	0003I	56	42	PW	PW	0·75
	0005I	70	70	PW	PW	1·00
				Average		0·96
				Standard deviation		0·084
				Coefficient of variation		8·7%

†S = splitting; PW = planar wedging; OPW = out-of-plane wedging; LF = lower failure.

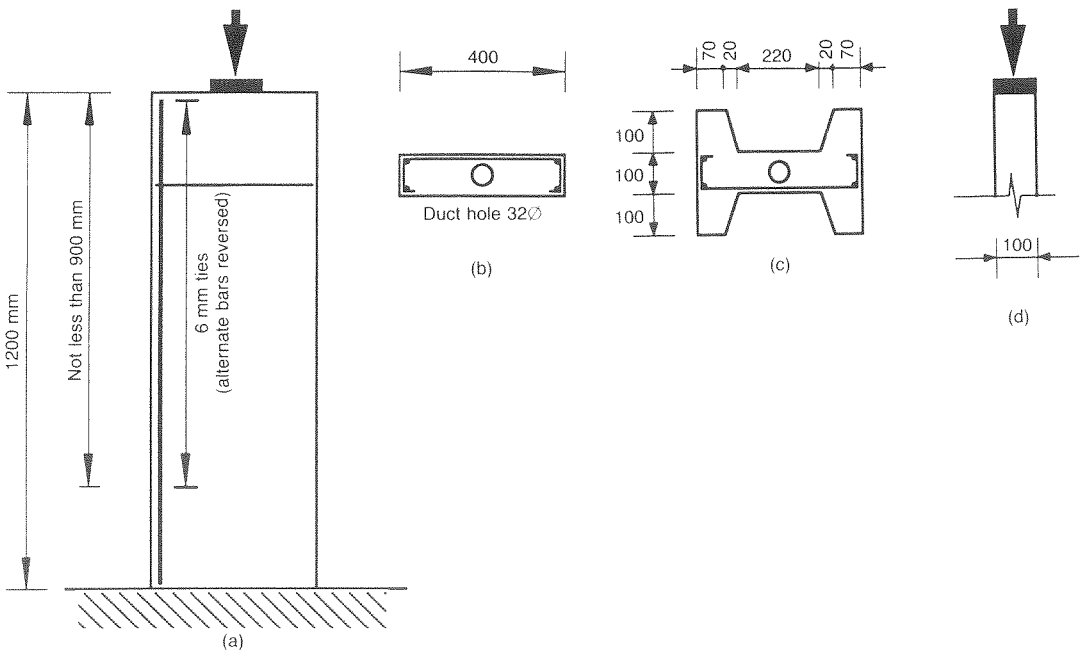

Fig. 13. Ref. 9 test specimens, showing details of geometry, reinforcing arrangements and loading: (a) overall specimen dimensions; (b) rectangular section; (c) I-section; (d) section through loading plate

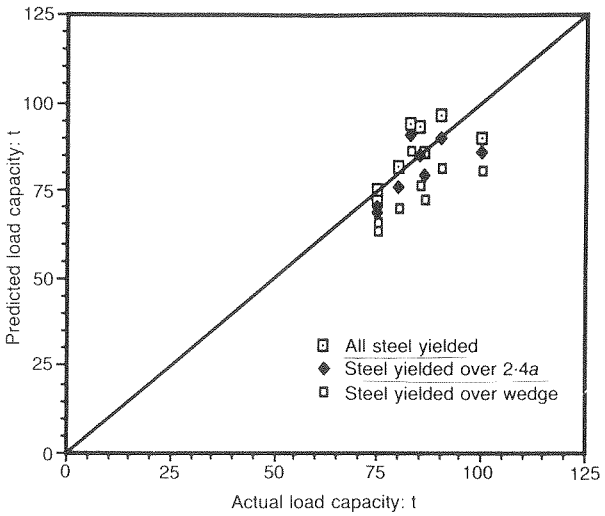

Fig. 14. Correlation of Ref. 9 test results and predictions of the present method of analysis

Figure 14 shows a plot of the correlation between test results and predicted ultimate load capacities of the prisms, under the various steel stress assumptions. Correlation is reasonably good, particularly when it was assumed either that steel had yielded over a depth $2 \cdot 4a$ or that all steel had yielded. It appears unreasonable, therefore, to assume that only the steel reinforcement over the depth of the wedge yields. Furthermore, assuming that steel *outside* the failure zone has yielded is unlikely to alter the stress distribution *inside* the failure zone significantly, since the steel forces consist simply of opposing equal forces.

Agreement between the present method of analysis and strip-loading test data has been reasonably good. It appears that strength of concrete and geometry of specimen are modelled in a fairly accurate manner.

Example

In order to illustrate the practicality of the above method fully, an example of the design of an anchorage zone is analysed here. The example is taken from Ref. 10. Fig. 15 shows the final design of the web steel, as recommended in the design guide, based on every anchorage carrying 223 t. Fig. 16 shows the model used to predict the strength of such an anchorage zone. Since the anchors are very close together in the webs, they have been combined into a single anchor, as suggested in Ref. 10. In the absence of more information, it has been assumed that the cube strength of the concrete is $f_{cu} = 50$ N/mm^2.

Using the present analysis technique, it is predicted that planar wedging failure in the webs will occur at a load of 562 t in each anchorage, assuming that all steel, positioned to counteract bursting, yields. However, it is predicted that out-of-plane failure will occur in the webs at a load of 408 t in each anchorage if no steel is positioned to counteract this failure. From a third analysis of the anchor zone, it was found that it would be necessary to position seven closed stirrups (or helices) of bar type Y16 around each anchor to prevent out-of-plane failure occurring before planar wedging failure.

Therefore, although the anchorage zone in the example clearly appears to be safe, the mode of failure of the zone might differ from the one that was assumed during design. Thus, it is recommended that designers satisfy themselves

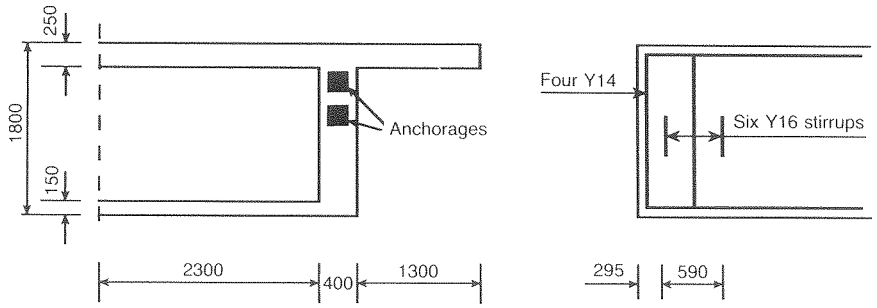

Fig. 15. Example from Ref. 10: dimensions in millimetres

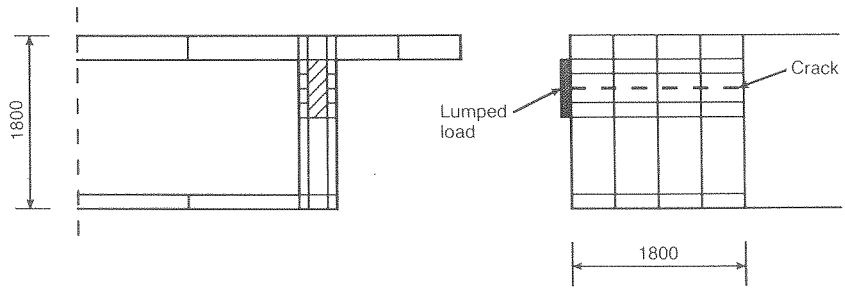

Fig. 16. FE layout for Ref. 10 example

fully that the failure of anchorage zones can occur only in the mode assumed in their design.

Conclusions

It has been found that the use of 2-D FEs, in combination with a plasticity failure criterion for concrete, models reasonably the problem of strip-loaded concrete prisms. Ultimate wedging failure is predicted adequately, assuming that the steel reinforcement has yielded along the failure planes.

In the experimental test series of Ref. 1, third-direction failure of some specimens occurred. It was therefore decided to model the problem using 3-D FEs, and to study the possibility of out-of-plane failure. Such analyses were found to predict the type of behaviour and the ultimate load capacity of each particular prism reasonably well. These specimens were of varying concrete strengths and reinforced to varying degrees.

A design example of an anchorage zone has shown that out-of-plane failure is possible in anchorage zones where planar behaviour has been assumed. Although such failure is predicted to occur at loads well above the design capacity, it is important that the designer be satisfied that all possible failure modes have been considered, lest the relevance of the original analysis be lost.

References

1. IBELL T. J. and BURGOYNE C. J. An experimental investigation of the behaviour of anchorage zones. *Mag. Concr. Res.*, 1993, **45**, 281–292.
2. IBELL T. J. and BURGOYNE C. J. A plasticity analysis of anchorage zones. *Mag. Concr. Res.*, 1994, **46**, No. 166, 39–48.
3. IBELL T. J. *Behaviour of anchorage zones for prestressed concrete*. University of Cambridge, PhD dissertation, 1992.
4. NIELSEN M. P. *Limit analysis and concrete plasticity*. Prentice-Hall, Englewood Cliffs, NJ, 1984.
5. HOFBECK J. A. *et al.* Shear transfer in reinforced concrete. *J. Am. Concr. Inst.*, 1969, 66-13, Feb., 119–128.
6. JENSEN B. C. Lines of discontinuity for displacements in the theory of plasticity of plain and reinforced concrete. *Mag. Concr. Res.*, 1975, **27**, No. 92, Sept., 143–150.
7. YETTRAM A. L. and ROBBINS K. Anchorage zone stresses in axially post-tensioned members of uniform rectangular section. *Mag. Concr. Res.*, 1969, **21**, No. 67, June, 103–112.
8. NIYOGI S. K. Bearing strength of concrete — geometric variations. *J. Struct. Engng Div. Am. Soc. Civ. Engrs*, 1973, **99**, ST7, July, 1471–1490.
9. FENWICK R. C. and LEE S. C. Anchorage zones in prestressed concrete members. *Mag. Concr. Res.*, 1986, **38**, No. 135, June, 77–89.
10. VSL INTERNATIONAL. *End block design in post-tensioned concrete*. Berne, 1975.

Discussion contributions on this Paper should reach the Editor by 30 December 1994